ORIGINAL ARTICLE

Impact of Image Reconstruction on Quantitative Analysis of 18F-FDG PET in Epilepsy Evaluation: A Preliminary Study

Naghmeh Firouzi [1, 2], **Ali Asghar Parach** [3], **Kaveh Tanha** [4], **Mohammad Sadegh Rostami** [5], **Parham Geramifar** [6*]

[1] Department of Medical Physics, School of Medicine, Shahid Sadoughi University of Medical Sciences, Yazd, Iran

[2] Research Center for Molecular and Cellular Imaging, Advanced Medical Technologies and Equipment Institute, Tehran University of Medical Sciences, Tehran, Iran

[3] Institut de Recherche en Cancérologie de Montpellier, INSERM U1194 – ICM, France

[4] Department of Medical Physics and Biomedical Engineering, School of Medicine, Tehran University of Medical Sciences, Tehran, Iran

[5] Faculty of Psychology, Tarbiat Modarres University, Tehran, Iran

[6] Research Center for Nuclear Medicine, Shariati Hospital, Tehran University of Medical Sciences, Tehran, Iran

*Corresponding Author: Parham Geramifar
Email: pgeramifar@tums.ac.ir

Abstract

Purpose: In epilepsy pre-surgical evaluations, semi-automated quantitative analysis of Fluorine-18-fluorodeoxyglucose (^{18}F-FDG) brain PET complements visual assessment for localizing the seizure onset zone. This study evaluates how adjusting reconstruction parameters enhances quantitative accuracy, aiming to identify optimal configurations for reliable clinical decision-making.

Materials and Methods: 234 reconstruction methods were applied to ^{18}F-FDG brain PET images of a 47-year-old male with focal epilepsy. The parameters encompassed the 3D-Ordered-Subset Expectation Maximization image reconstruction method, both with Resolution Recovery (RR) and without (non-RR), various numbers of iterations×subset (#it×sub), pixel sizes, and Gaussian filters. The accuracy errors were determined by the Relative Difference Percentage (RDP) in measured maximum standardized uptake value SUV_{max} and absolute Z-scores from all 234 reconstructed images, compared to reference values from the normal database reconstruction set as the benchmark

Results: The study revealed that reconstructed images with 5 mm or 8 mm full width at half maximum (FWHM) Gaussian filters yielded RDP values above 5% for SUV_{max} and Z-scores, indicating potential inaccuracy with higher values of post-smoothing filters. The recommended reconstruction sets with RDP values below 5% for both RR and non-RR images were those with a 3 mm FWHM Gaussian filter and higher (#it×sub), specifically (5×21, 8×21), (5×21, 6×21), and (7×21, 8×21) for pixel sizes of 1.01 mm, 1.35 mm, and 2.03 mm, respectively.

Conclusion: The findings underscore the significant impact of altering the image reconstruction sets on the SUVmax and Z-scores. Furthermore, the inconsistent fluctuations of Z-scores emphasize the importance of using standardized image reconstruction sets to ensure accurate and reliable quantitative outcomes in epilepsy pre-surgical evaluations.

Keywords: Positron Emission Tomography; Fluorine-18-fluorodeoxyglucose; Drug-Resistant Epilepsy, Image Reconstruction.

1. Introduction

Epilepsy, characterized by unprovoked and recurrent seizures, is among the most prevalent neurological disorders, affecting approximately 46 million people globally. It significantly impacts patients' quality of life, particularly in resource-limited settings [1-3]. The Task Force of the International League Against Epilepsy (ILAE) defines medical refractory, intractable, or Drug-Resistant Epilepsy (DRE) as patients who do not respond successfully to two or three pharmacological treatments with no specific reason [4, 5]. Surgical intervention might be a beneficial treatment method for DRE patients, which may reduce future seizure attacks and improve their overall health [5]. It is estimated that one in three 20–30% of all patients who have epilepsy are referred for surgical resection following pre-surgical Seizure Onset Zone (SOZ) localization procedures such as Video-Electroencephalography (V-EEG) or Magnetic Resonance Imaging (MRI) of the brain [6, 7]. The VEEG is a gold standard test for seizure type classification [8], specifically for distinguishing patients with Psychogenic Non-Epileptic Seizures (PNES) who do not respond to medication, including 25-40% of DRE patients. Surgery, particularly in patients with lesional temporal epilepsy, has demonstrated the best efficacy [9].

The post-surgical remission rate is also high in patients with non-lesional temporal lobe epilepsy [10]. At the same time, there is a high concordance of SOZ localization between Electroencephalography (EEG) and other imaging modalities such as Positron Emission Tomography (PET), Single-Photon Emission Computerized Tomography (SPECT), or mass spectrometry imaging (MSI). Moreover, if there is an agreement between Magnetic Resonance Imaging (MRI) and EEG in SOZ evaluations, neocortical focal epilepsy has demonstrated the highest response rate to surgical intervention [11]. However, SOZ localization by other modalities, such as PET, SPECT, or MSI, can lead to a remission rate higher than 50 percent [11]. If noninvasive procedures for SOZ locations remain inconclusive, invasive approaches such as intracranial electro-Encephalography (iEEG) evaluations might be required [11]. When considering surgery as a treatment choice, it is essential to localize the epileptogenic spots accurately to achieve the best outcomes. Most patients with epilepsy disorder require a brain MRI to assess possible structural abnormalities.

Regarding the benefits of MRI, such as higher sensitivity, better soft-tissue contrast, and spatial resolution compared to Computed Tomography (CT), it is currently the mainstay of neuroimaging in epilepsy disorders [12, 13]. However, reliable epileptogenic MRI evaluations require high expertise and sophisticated protocols not commonly available in less specialized centers [13]. Additionally, MRI generally detects brain atrophy in advanced stages of epilepsy, while functional changes may occur much earlier and can be identified using Fluorine-18-Fluorodeoxyglucose (^{18}F-FDG) brain PET imaging [14, 15]. For the last two decades, ^{18}F-FDG PET imaging has been extensively used to evaluate the regional functional features of brain patients with seizure disorders, improving the SOZs localization [6, 16], and as a supplement to structural imaging when they remain controversial and no conclusive results [17, 18]. The contribution of ^{18}F-FDG PET to the localization of SOZ is vital to achieving successful resection surgery [19] because MRI or intracranial EEG might not be contributory in 15-30% of patients with refractory epilepsy [6, 7, 20].

Visual-based assessment is routinely used clinically to interpret ^{18}F-FDG brain PET images and SOZ localization [21]. It not only depends on the knowledge and experience of the observer but also relies on the quality of the images, specifically where there is a subtle abnormal spot that could make it hard to distinguish [21, 22]. Using semi-automated quantitative analysis software is a supplementary approach to enhance accuracy and confidence in decision-making for localizing epileptogenic regions [23, 24].

Brain metabolism quantification commonly employs two techniques: Region Of Interest (ROI) analysis and voxel-based analysis. These techniques can be employed together or independently, depending on the specific research or clinical needs [25]. The voxel-wise statistics method involves the automated alignment of brain scans with a specific template for voxel or pixel-based sampling [26]. It is crucial to mention that achieving accurate localization

of intricate brain structures strongly relies on image quality [27], which can be significantly influenced by image reconstruction parameters. Moreover, the accuracy of the quantitative values obtained from the software can be affected by various factors, including image reconstruction sets [28, 29]. The iterative method is commonly used for solving problems that require optimization. It works by performing a series of steps that gradually improve the match between the measured data (projections) and the estimated reconstruction. In image reconstruction, some methods process smaller groups of projections (called subsets) in each step. One widely used algorithm in this category is the Ordered Subset Expectation Maximization (OSEM), which is highly popular due to its effectiveness [30].

This study explores the impact of altering these sets on the quantitative values provided by the software. To this aim, the OSEM reconstruction methods with resolution recovery (RR) and without (non-RR) were implemented on the images. Various parameters such as the size of Gaussian filters (used to smooth images by reducing the noise) [31], number of iterations×subset (#it×sub), and different pixel sizes were systematically analyzed to evaluate their effect on quantitative results, including the maximum standardized uptake value (SUV_{max}) and Z-scores. SUV_{max} was chosen because it shows the highest level of activity in a region, making it better for detecting small or specific abnormalities. Unlike SUV_{mean}, which provides an average value that can be influenced by the clinician's expertise in defining the region of interest, SUV_{max} is less dependent on precise contouring. Additionally, SUV_{mean} can miss important details in areas with mixed activity. For this study, focusing on precise and localized abnormalities was essential, so SUV_{max} was selected.

Our hypothesis was based on the idea that the semi-automated quantitative analysis of ^{18}F-FDG brain PET images, used in the presurgical evaluations of DRE patients, might be influenced by the image reconstruction parameters.

We aimed to investigate whether modifying common image reconstruction settings could significantly impact the SUV_{max} and Z-scores. To evaluate this, we compared the results obtained with these altered settings to the values provided by the

image reconstruction set used by the software's normal database, which we considered the reference.

This study introduces a novel approach to optimizing ^{18}F-FDG brain PET imaging for precise Seizure Onset Zone (SOZ) localization in DRE. By systematically assessing how image reconstruction parameters—such as Gaussian filter size, pixel size, and iterative settings—affect quantitative metrics like Z-scores and SUV_{max}, it highlights the significant impact of these settings on diagnostic accuracy. The findings provide valuable recommendations for improving PET imaging reliability in pre-surgical assessments, ultimately enhancing clinical outcomes for DRE patients.

2. Materials and Methods

2.1. Patient's Characteristics and Imaging Procedure

This preliminary study seeks to highlight an issue that requires further investigation. The current study delves into the influence of image reconstruction configurations on quantitative metrics within cerebral PET images, a critical facet for precise preoperative assessments among individuals with DRE. This cross-sectional retrospective study examined the patient's ^{18}F-FDG brain image of a patient, acquired using a Biograph Truepoint PET/CT scanner (Siemens Healthcare, Erlangen, Germany). We utilized an ^{18}F-FDG brain PET image of a 47-year-old male patient with refractory epilepsy. The image shows a hypo metabolism spot in his Left Frontal Lobe (LFL). Informed consent had been obtained from the participant, and the ethics approval code was IR.SSU.MEDICINE.REC.1395.293.

The PET images were attenuation-corrected using low-dose CT images (130 kV, 90 mAs). It is worth noting that systematic patient preparation and careful head positioning, aimed at minimizing motion artifacts, significantly impacted the image quality and subsequent quantitative results. Consequently, all necessary measures to minimize systematic errors were carefully employed. 370 MBq ^{18}F-FDG was administered to the patient, who had to rest for 40 minutes in a dimly lit room, and a 10-minute PET/CT brain protocol acquisition was implemented. The standard reconstructed image matrix was 336 × 336,

with a 1.08 mm size of pixel size and 3 mm slice thickness.

To obtain brain images of satisfactory quality, we followed a precise brain protocol. We employed two iterative reconstruction methods: one with resolution recovery, referred to as RR (Resolution Recovery) images, and another without resolution recovery, referred to as non-RR images. In this context, we examined three different sizes of Gaussian filters: 3, 5, and 8 mm full width at half maximum (FWHM). Additionally, we explored combinations of iterations (it) and subsets (sub), including 1, 2, 3, 4, 5, 6, 7, and 8 iterations with 8, 16, and 21 subsets. In addition, three distinct pixel sizes—1.01 mm, 1.35 mm, and 2.03 mm—were employed during the reconstruction process. In total, 234 reconstruction sets were applied to the ^{18}F-FDG brain image. Table 1 summarizes the investigated reconstruction sets with various numbers of iterations and subsets, post-smoothing Gaussian filters, and PET image pixel sizes in RR and non-RR image reconstruction methods.

Quantitative analyses were conducted using Scenium software (Siemens CTI molecular imaging, Knoxville, TN, USA), a semi-automated tool for quantitative brain analysis. The software generated statistical color-coded images displaying Z-score values, representing the number of standard deviations from the mean. Additionally, Scenium provided measurements such as SUV_{max}, minimum standardized uptake value (SUV_{min}), mean standardized uptake value (SUV_{mean}), and related standard deviations. Furthermore, the software provided seven normal brain databases, each varying in terms of scanner types, reconstruction parameters, and age ranges of participants. Given that the patient underwent ^{18}F-FDG brain PET imaging using the Biograph Truepoint PET/CT scanner, we specifically utilized three categories of the software's normal databases provided by this scanner. These categories possess the following distinct characteristics:

1) Thirty-three normal individuals (ages 46 to 79) were scanned with the Biograph Truepoint PET/CT scanner, employing three-dimensional Ordered Subset Expectation Maximization (OSEM3D) reconstruction, normalization based on whole brain structures, and a 12 mm FWHM Gaussian filter.

2) Thirty-three normal individuals (ages 46 to 79) were scanned with the Biograph Truepoint PET/CT scanner, employing OSEM3D-RR reconstruction, normalization based on whole brain structures, and a 12 mm FWHM Gaussian filter.

3) Thirty-eight normal cases (ages 19 to 44) were scanned with the Biograph Truepoint PET/CT scanner, employing OSEM3D reconstruction and normalization based on whole brain structures without a smoothing filter.

Considering the patient's age range, we implemented the first two groups of the above databases as normal ^{18}F-FDG brain PET templates. Two categories of iterative OSEM3D reconstruction parameters were applied for normal databases presented by the software, which we considered as a reference to assess and compare the quantitative results, including Z-scores and SUV_{max}:

1) For non-RR OSEM3D: 336×336 Matrix, zoom 2, 6 iterations, 21 subsets, 3 mm FWHM post-smoothing Gaussian filter.

In non-RR OSEM3D reconstruction, a lower number of iterations was applied to mitigate noise amplification, ensuring optimal signal-to-noise ratio and quantitative accuracy [32].

2) For RR OSEM3D: 336×336 Matrix, zoom 2, 8 iterations, 21 subsets, 3 mm FWHM post-smoothing Gaussian filter.

Table 1. Summary of investigated reconstruction parameters

Resolution Recovery	Gaussian Filter (mm)	Iteration and Subsets Combinations (it×sub)			Pixel Size (mm)
RR	3	1×8	2×16	2×21	1.01
non-RR	5	2×8	5×16	3×21	1.35
	8	3×8		4×21	2.03
		7×8		5×21	
				6×21	
				7×21	
				8×21	

In addition, the Z-score values were calculated by (Equation 1) as presented in the supplementary [33].

$$Z\_score = \frac{individual\ value - control\ mean}{control\ standard\ deviation} \quad (1)$$

2.1. Software's Quantification Procedure

2.1.1. Fusion to the Supporting CT Images

In conjunction with functional PET images, the supporting CT images play an important role in distinguishing closely located abnormalities and identifying their precise location. Since both the functional and anatomical scans are from the same patient, there is no need for stretching or deforming either scan. An experienced physician aligned the images for more accurate comparison and analysis.

The process involves identifying landmarks within the images and performing rigid registration of the functional and anatomical scans.

2.1.2. Fusion to the Normal Brain

The software's standard ROIs were defined based on a normal brain template. To align the patient's PET/CT image and its corresponding normal database human brain 'atlas', known as Talairach, A landmark registration method, validated by an expert physician, was employed. As a result, the ROIs were established on the patient's ^{18}F-FDG brain PET image. Precise image fusion was crucial for accurately localizing the ROIs and ensuring reliable analytical outputs.

2.1.3. Providing and Comparing the Quantitative Results

The following steps above obtained quantitative results for 134 brain regions using the software. Specifically, we evaluated the Z-scores and SUV$_{max}$ of the patient's LFL, which served as the abnormal hypo-metabolism brain region. To compare the quantitative results from different image reconstruction sets, we used reference values from images reconstructed with the standard parameters of the software's normal databases. The relative difference percentage (RDP) of SUV$_{max}$ was calculated using Equation 2.

$$Relative\ Difference\ Percentage = \frac{|a-b| \times 100}{b} \quad (2)$$

Where a and b are the measured and reference quantities, respectively. It should be noted that RDP values below 5 percent were considered acceptable in this study.

3. Results

All the investigated reconstruction parameters with calculated RDP values of SUVmax and Z-score compared with reference in RR and non-RR OSEM3D image reconstruction sets are presented in supplementary Tables A.2, A.3, and A.4. Using the non-RR reference image reconstruction set (6i21s, 3 mm FWHM Gaussian filter, and 1.01 mm pixel size), the SUV$_{max}$ and Z-score values were measured as 18.15 and -2.9, respectively. Furthermore, for the RR image reconstructed using the reference reconstruction set (8i21s, 3 mm FWHM Gaussian filter, and 1.01 mm pixel size), the SUV$_{max}$ and Z-score values were measured as 20.83 and -2.7, respectively.

Figure 1 displays the patient's SUV images, highlighting the influence of various (#it×sub) with a 3 mm FWHM post-smoothing Gaussian filter on RR and non-RR images with pixel sizes of 1.01 mm. Moreover, Figure 2 shows two 3D-stereotactic surface projections (3D-SSPs) [33, 34] of Z-Score images reconstructed using the reference setting (6i21s, 3 mm FWHM Gaussian post-smoothing filter and 1.01 mm pixel size) and an alternative reconstruction setting (8i21s, 3 mm FWHM Gaussian post-smoothing filter and 1.01 mm pixel size).
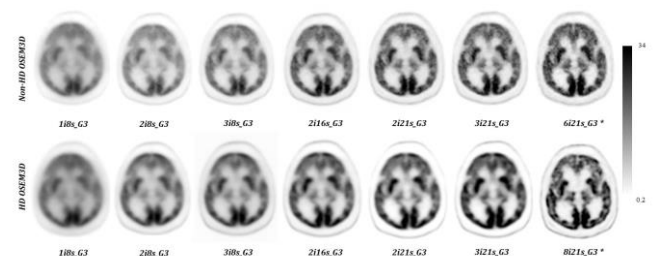

Figure 1. ^{18}F-FDG brain PET images with different image reconstruction sets with a 3 mm FWHM post-smoothing Gaussian filter and pixel sizes of 1.01 mm. The non-RR OSEM3D Images (Up row) and RR OSEM3D images (Bottom row).*: Reconstructed image with reference reconstruction set

Figure 3 presents an overview of the SUV$_{max}$ obtained from various image reconstruction settings compared to the reference values derived from the normal database reconstruction set used as the benchmark for RR and non-RR images.
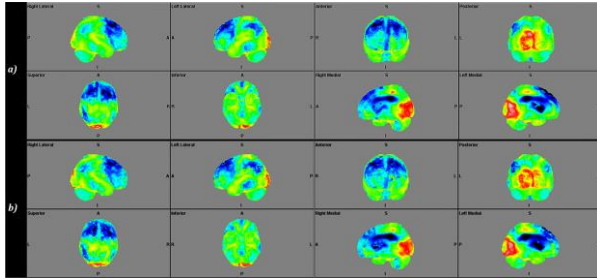

Figure 2. Patient's 3D-stereotactic surface projections z-score of nonRR-OSEM3D images reconstructed by (a) reference reconstruction settings (6i21s, 3 mm FWHM Gaussian post smoothing filter, and 1.01 mm pixel size) and (b) different reconstruction settings of 8i21s, 1.01 mm pixel size, and 8 mm FWHM Gaussian post-smoothing filter
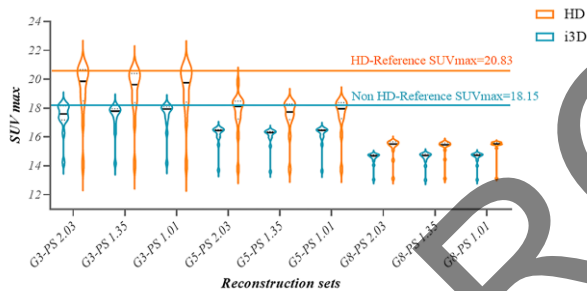

Figure 3. SUV$_{max}$ is derived from the patient's ^{18}F-FDG brain PET image data. GN: Gaussian filter with N mm FWHM. PS: Pixel Size (mm). Reference value derived from the normal database reconstruction set used as the benchmark

Figures 4 and 5 display the heatmaps of RDP values for SUV$_{max}$ and Z-score calculated for reconstructed PET images using different settings. The heatmaps illustrate RDP values as a grid of colored squares, plotted against pixel size, Gaussian filter, and (#it×sub) variables.

4. Discussion

PET imaging is a widely utilized functional imaging modality for the pre-surgical assessment of DRE patients [34, 35]. In interictal periods, the epileptogenic regions in ^{18}F-FDG brain PET images exhibit reduced glucose metabolism [36]. The widely used visual assessment of images in clinical centers
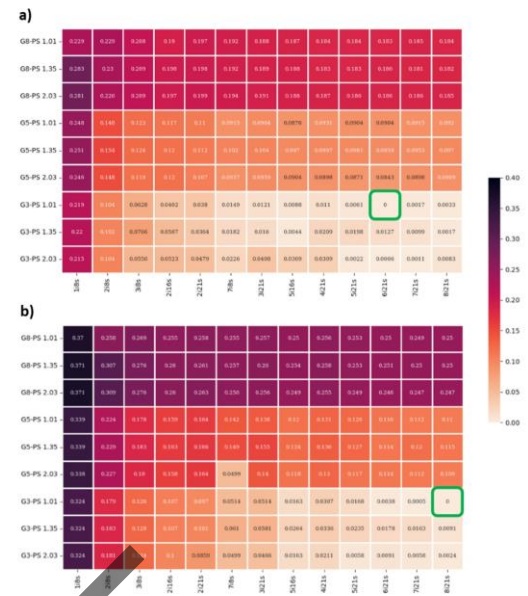

Figure 4. The relative difference percentage value of SUV$_{max}$ in various image reconstruction sets in (a) non-RR OSEM3D image reconstructions with the green box as the reference (6i21s, 3 mm FWHM and pixel size= 1.01 mm), (b) RR OSEM3D image reconstructions with the green box as the reference (8i21s, 3 mm FWHM and pixel size= 1.01 mm). GN: Gaussian filter with N mm FWHM. PS: pixel size (mm). All values are rounded to the nearest five percent

Figure 5. The relative difference percentage value of Z-Scores in various image reconstruction sets in (a) non-RR OSEM3D image reconstructions with the green box as the reference (6i21s, 3 mm FWHM, and pixel size= 1.01 mm) (b) RR OSEM3D image reconstructions with the green box as the reference (8i21s, 3 mm FWHM, and pixel size= 1.01 mm). GN: Gaussian filter with N mm FWHM. PS: pixel size (mm). All values are rounded to the nearest five percent
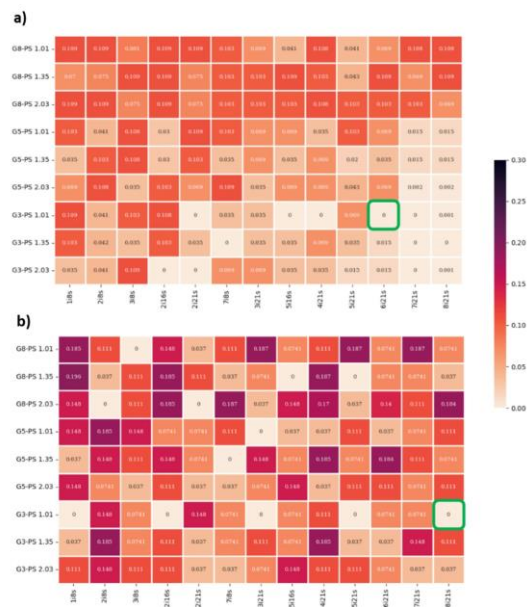
heavily relies on the physician's expertise and clinical diagnostic experience, which can significantly influence the identification of suspected zones [37]. Misinterpretation of pre-surgical evaluations in patients with DRE can lead to serious consequences, including omitting critical follow-up assessments or unnecessarily repeating medical evaluations, thereby imposing substantial costs on the patient while they continue to endure debilitating seizures. Furthermore, delays in surgical intervention can increase the disease burden and elevate the risks of morbidity and mortality, particularly when resective surgery is indicated [38]. Therefore, it is crucial to use quantitative methods to provide a more dependable diagnosis for the localization of SOZs [23]. However, integration of these advanced techniques in everyday clinical practice can be challenging, especially in less specialized centers. Limited access to the necessary tools and expertise makes their routine use difficult. To address this, there is a pressing need for enhanced training, standardized protocols, and access to advanced software for image reconstruction and analysis. Overcoming these barriers could make PET imaging more accurate and effective for presurgical evaluations in DRE patients. This study aimed to assess the impact of various image reconstruction parameters on the quantification of ^{18}F-FDG brain PET, focusing on the variability of Z-scores and SUV_{max}.

The accurate identification of abnormal regions can be affected by image quality, which heavily depends on the choice of reconstruction methods and parameters, as shown in Figure 1. The OSEM image reconstruction algorithm was selected for its ability to produce higher-quality images with an improved signal-to-noise ratio (SNR) and reduced streak artifacts, particularly in cases of PET images with poor statistical data [39, 40]. However, excessively high or low values for (#it×sub) can introduce noise and artifacts that negatively impact the quality of the reconstructed image [39, 41, 42]. Moreover, resolution recovery techniques in image reconstruction have demonstrated their ability to enhance image quality by optimizing spatial resolution, boosting image contrast, and lowering noise. Therefore, it can lead to greater diagnostic accuracy, better delineation of anatomical structures, and more reliable quantitative analyses across various medical imaging applications [43].

Figure 2 shows the substantial impact of image reconstruction sets on statistical color-coded images, which provide Z-score values. It is essential to emphasize the impact of deviations from the reference reconstruction settings, as they can lead to the exclusion of subtle abnormal regions from subsequent evaluations. In Figure 3, the SUV_{max} of images reconstructed using a 3 mm FWHM Gaussian filter and varying pixel sizes closely approximated the reference SUV_{max} for both RR and non-RR images. However, as the Gaussian filter size increased, these values progressively deviated from the reference quantities. Additionally, SUV_{max} derived from RR images was consistently higher than that from non-RR images.

As illustrated in Figure 4, increasing (#it×sub) in non-RR and RR OSEM3D image reconstruction sets reduced SUV_{max} fluctuations across different pixel sizes and post-smoothing Gaussian filters. Moreover, as demonstrated in Figure 4a, variations in SUV_{max}, associated with cells corresponding to the 3 mm FWHM Gaussian filter, remained within an acceptable error level (<5%) even when applying higher (#it×sub) than the reference level. Additionally, findings from Table A2 indicate that for non-RR images, RDP SUV_{max} values remained within the acceptable range (<5%) when (#it×sub) values were ≥32. For RR images, this threshold increased to (#it×sub) values ≥80. However, increasing the FWHM value of the post-smoothing Gaussian filters caused RDP values to exceed the ±5% range, indicating potential inaccuracies. Tables A3 and A4 further show that all reconstruction sets employing a 5 mm or 8 mm FWHM Gaussian filter exhibited RDP values exceeding 5% for SUV_{max} across all pixel sizes in both non-RR and RR images. These findings highlight the adverse effects of excessively increasing the smoothing filter size.

Figure 4b demonstrates that applying resolution recovery during the reconstruction process maintains SUV_{max} variations within acceptable error levels, similar to non-RR images, but at higher (#it×sub) values. For instance, when reconstructing images with a pixel size of 1.01 mm, the RDP value of SUV_{max} remained below 5% at (#it×sub) values of 32 and 80 for non-RR and RR images, respectively. However, increasing the pixel size to 2.03 mm shifted these values to 42 and 56, respectively. As illustrated in

Figure 4, image reconstruction sets using 5 mm and 8 mm FWHM Gaussian filters should not be considered, regardless of the iterations, subsets, or pixel sizes. Conversely, reconstruction sets with a 3 mm FWHM Gaussian filter displayed acceptable SUV_{max} error levels across all three pixel sizes when (#it×sub) values exceeded 32 for non-RR images and 56 for RR images.

As shown in Figure 5, error levels generally decreased in non-RR image reconstruction sets when smaller FWHM values of Gaussian filters were combined with higher (#it×sub) values. In contrast, the RDP values of Z-scores in RR images did not demonstrate regular or consistent patterns with increasing iterations and subsets (#it×sub), as illustrated in Figure 5.b. Z-scores are among the most critical quantitative metrics, particularly for identifying group abnormalities or performing longitudinal studies. The weaker correlation for the relative difference of Z-scores happens because Z-scores are more sensitive to small changes in reconstruction settings and noise. Unlike SUV_{max}, which measures peak activity, Z-scores compare voxel activity to a normal database. This process can amplify small variations, especially in non-RR reconstructions where noise is higher. Additionally, the way Z-scores are normalized can cause inconsistencies, leading to less clear patterns in the heatmap. When localizing SOZs using ^{18}F-FDG brain PET images, even slight biases in Z-scores can significantly impact evaluations. These biases may lead to false positives or false negatives in identifying epileptogenic sites, resulting in either the exclusion of suspected hypometabolism zones from further preoperative evaluations or the incurrence of unnecessary costs for ineffective assessments. Z-scores below -2 indicate abnormal hypometabolism zones, potentially signifying SOZs, while Z-scores above -2 represent normal regions. Slight deviations across this threshold can severely affect outcomes, particularly in evaluations conducted by individuals with limited experience or expertise.

Given the critical role of accurate Z-scores in SOZs localization, our findings underscore the importance of using reconstruction parameters aligned with those provided in the software's normal database. This is especially pertinent when resolution recovery techniques are applied, ensuring reliable and precise preoperative evaluations.

A notable observation was the significantly lower number of acceptable reconstruction sets (RDP values of $SUV_{max} < 5\%$) in RR images compared to non-RR images. For non-RR images, increasing the pixel size led to an increase in acceptable reconstruction sets from 46% to 70% of the total. In contrast, for RR images, the proportion decreased from 38% to 30%.

Importantly, none of the reconstructed images using 5 mm or 8 mm FWHM Gaussian filters achieved RDP values of less than 5% for both SUV_{max} and Z-scores. These findings indicate that using 5 or 8 mm FWHM post-smoothing Gaussian filters does not yield accurate measurements.

The only (#it×sub) sets with RDP values below 5% for both SUV_{max} and Z-scores in RR and non-RR images were obtained exclusively with the 3 mm Gaussian filter. These acceptable sets included (5×21, 8×21), (5×21, 6×21), and (7×21, 8×21) for pixel sizes of 1.01 mm, 1.35 mm, and 2.03 mm, respectively.

Previous studies have looked at how reconstruction settings affect PET images, especially in cancer and brain studies. Yan *et al.* (2015) found that changes in reconstruction settings impact features like texture in PET images, which is similar to our findings on SUV_{max} and Z-scores. However, while their study focused on cancer imaging, our research looks at epilepsy, specifically how these settings affect seizure onset zone localization in epilepsy evaluations [28].

In addition, Kuntner and Stout (2014) discussed how important it is to balance noise and resolution in PET imaging for research, which matches our finding that reconstructions with fewer iterations have lower noise but less detail. Our study builds on this by offering recommendations for reconstruction settings in clinical epilepsy imaging, stressing the need for standardized protocols to improve diagnosis accuracy [44].

As of December 2024, our comprehensive search using the keywords "Drug Resistant Epilepsy", "Image Reconstruction", "PET", and "Epilepsy" in papers' titles yielded no other relevant studies. This study provides a novel approach to optimizing ^{18}F-FDG brain PET imaging for the precise localization of SOZs in patients with DRE. By systematically evaluating the impact of various image reconstruction

parameters—such as Gaussian filter size, pixel size, and iterative reconstruction settings—on quantitative measures like Z-scores and SUV_{max}, this research offers new insights into how to improve the accuracy of PET imaging for pre-surgical assessments. The findings highlight that deviations from standard reconstruction settings can significantly affect diagnostic accuracy, which is crucial for clinical decision-making. This work contributes to a better understanding of the impact of reconstruction methods and provides recommendations for enhancing the reliability of PET imaging, ultimately improving patient outcomes by ensuring more accurate localization of SOZs.

4.1. Study Limitation

Although this is a preliminary study, addressing its limitations can improve the quality of our work. First, the study relied on data from a single patient, which may not fully represent the diverse cases encountered in clinical practice. Second, the use of Scenium software for quantitative analysis introduces the potential for software-specific biases. Different software tools in the field may utilize distinct algorithms and reconstruction methods, potentially leading to varying results. Additionally, future studies could investigate the impact of different PET scanner models or imaging protocols on reconstruction results. While this study focused on DRE, exploring the applicability of these methods to other conditions, such as Alzheimer's disease, Parkinson's disease, or traumatic brain injury, could further enhance their relevance and utility.

5. Conclusion

Quantitative analysis of ^{18}F-FDG brain PET images is commonly used for precise localization of the SOZs. However, it is crucial to ensure that the image reconstruction parameters align with the normal database reference set to achieve accurate quantitative results, particularly Z-scores. Any deviations from this reference can significantly impact the clinical interpretation of the results. Misinterpretation of pre-surgical evaluations in DRE can lead to missed follow-ups, unnecessary costs, and delays in surgery, ultimately increasing patient risks. Therefore, it is essential to exercise caution when using parameters

other than those in the benchmark reconstruction set to ensure improved accuracy in quantitative outcomes.

References

1- Ettore Beghi, "The epidemiology of epilepsy." *Neuroepidemiology,* Vol. 54 (No. 2), pp. 185-91, (2020).

2- William H Theodore, "Presurgical Focus Localization in Epilepsy: PET and SPECT." in *Seminars in nuclear medicine*, (2017), Vol. 47 (No. 1): *Elsevier*, pp. 44-53.

3- David J Thurman *et al.*, "The burden of premature mortality of epilepsy in high-income countries: a systematic review from the Mortality Task Force of the International League Against Epilepsy." *Epilepsia,* Vol. 58 (No. 1), pp. 17-26, (2017).

4- Wolfgang Löscher, Heidrun Potschka, Sanjay M Sisodiya, and Annamaria Vezzani, "Drug resistance in epilepsy: clinical impact, potential mechanisms, and new innovative treatment options." *Pharmacological reviews,* Vol. 72 (No. 3), pp. 606-38, (2020).

5- Johan Bjellvi, Ingrid Olsson, Kristina Malmgren, and Karin Wilbe Ramsay, "Epilepsy duration and seizure outcome in epilepsy surgery: A systematic review and meta-analysis." *Neurology,* Vol. 93 (No. 2), pp. e159-e66, (2019).

6- Stefan E Poirier *et al.*, "An evaluation of the diagnostic equivalence of 18F-FDG-PET between hybrid PET/MRI and PET/CT in drug-resistant epilepsy: A pilot study." *Epilepsy Research,* Vol. 172p. 106583, (2021).

7- Jorge G Burneo, Raymond Poon, Sarah Kellett, and O Carter Snead, "The utility of positron emission tomography in epilepsy." *Canadian Journal of Neurological Sciences,* Vol. 42 (No. 6), pp. 360-71, (2015).

8- Jukka Peltola *et al.*, "Semiautomated classification of nocturnal seizures using video recordings." *Epilepsia,* (2022).

9- George W Culler IV and Barbara C Jobst, "Surgical Treatments for epilepsy." *CONTINUUM: Lifelong Learning in Neurology,* Vol. 28 (No. 2), pp. 536-58, (2022).

10- Gregory D Cascino and Benjamin H Brinkmann, "Advances in the Surgical Management of Epilepsy: Drug-Resistant Focal Epilepsy in the Adult Patient." *Neurologic clinics,* Vol. 39 (No. 1), pp. 181-96, (2021).

11- Giridhar P Kalamangalam and Nitin Tandon, "Stereo-EEG implantation strategy." *Journal of Clinical Neurophysiology,* Vol. 33 (No. 6), pp. 483-89, (2016).

12- Yun Jeong Lee, "Advanced neuroimaging techniques for evaluating pediatric epilepsy." *Clinical and experimental pediatrics,* Vol. 63 (No. 3), p. 88, (2020).

13- Andrea Bernasconi *et al.*, "Recommendations for the use of structural magnetic resonance imaging in the care of patients with epilepsy: a consensus report from the International League Against Epilepsy Neuroimaging Task Force." *Epilepsia,* Vol. 60 (No. 6), pp. 1054-68, (2019).

14- Jonah Peter, Sina Houshmand, Thomas J Werner, Domenico Rubello, and Abass Alavi, "Novel assessment of global metabolism by 18F-FDG-PET for localizing affected lobe in temporal lobe epilepsy." *Nuclear medicine communications,* Vol. 37 (No. 8), pp. 882-87, (2016).

15- Jonah Peter, Mohsen Khosravi, Thomas J Werner, and Abass Alavi, "Global temporal lobe asymmetry as a semi-quantitative imaging biomarker for temporal lobe epilepsy lateralization: A machine learning classification study." *Hell. J. Nucl. Med,* Vol. 21pp. 95-101, (2018).

16- Javier Aparicio *et al.*, "Combined 18F-FDG-PET and diffusion tensor imaging in mesial temporal lobe epilepsy with hippocampal sclerosis." *NeuroImage: Clinical,* Vol. 12pp. 976-89, (2016).

17- Manohar Kuruva, Valeria M Moncayo, and Ryan B Peterson, "PET and SPECT imaging of epilepsy: technical considerations, pathologies, and pitfalls." in *Seminars in Ultrasound, CT and MRI*, (2020), Vol. 41 (No. 6): *Elsevier*, pp. 551-61.

18- Aldo Moro-AOU Policlinic, "Typical and atypical PET/CT findings in non-cancerous conditions." *Hellenic Journal of Nuclear Medicine,* (2020).

19- Maria Mayoral *et al.*, "Epileptogenic zone localization with 18FDG PET using a new dynamic parametric analysis." *Frontiers in Neurology,* Vol. 10p. 380, (2019).

20- John S Duncan, Gavin P Winston, Matthias J Koepp, and Sebastien Ourselin, "Brain imaging in the assessment for epilepsy surgery." *The Lancet Neurology,* Vol. 15 (No. 4), pp. 420-33, (2016).

21- Jonah Peter, Sina Houshmand, Thomas J Werner, Domenico Rubello, and Abass Alavi, "Applications of global quantitative18F-FDG-PET analysis in temporal lobe epilepsy." *Nuclear medicine communications,* Vol. 37 (No. 3), pp. 223-30, (2016).

22- Dongyan Wu *et al.*, "Characterizing the hyper-and hypometabolism in temporal lobe epilepsy using multivariate machine learning." *Journal of Neuroscience Research,* (2021).

23- Vanessa Cristina Mendes Coelho *et al.*, "Automated Online Quantification Method for 18F-FDG Positron Emission Tomography/CT Improves Detection of the Epileptogenic Zone in Patients with Pharmacoresistant Epilepsy." (in English), *Frontiers in Neurology,* Original Research Vol. 8 (No. 453), 2017-September-01 (2017).

24- P. Fu *et al.*, "NeuroGam Software Analysis in Epilepsy Diagnosis Using 99mTc-ECD Brain Perfusion SPECT Imaging." *Med Sci Monit,* Vol. 21pp. 2801-8, (2015).

25- Evangeline Yee, Karteek Popuri, Mirza Faisal Beg, and Alzheimer's Disease Neuroimaging Initiative, "Quantifying brain metabolism from FDG-PET images into a probability of Alzheimer's dementia score." *Human brain mapping,* Vol. 41 (No. 1), pp. 5-16, (2020).

26- Bianca De Blasi *et al.*, "Age-specific 18F-FDG image processing pipelines and analysis are essential for individual mapping of seizure foci in pediatric patients with intractable epilepsy." *Journal of Nuclear Medicine,* Vol. 59 (No. 10), pp. 1590-96, (2018).

27- Li Sze Chow and Raveendran Paramesran, "Review of medical image quality assessment." *Biomedical signal processing and control,* Vol. 27pp. 145-54, (2016).

28- Jianhua Yan *et al.*, "Impact of image reconstruction settings on texture features in 18F-FDG PET." *Journal of Nuclear Medicine,* Vol. 56 (No. 11), pp. 1667-73, (2015).

29- Nicolas Aide, Charline Lasnon, Patrick Veit-Haibach, Terez Sera, Bernhard Sattler, and Ronald Boellaard, "EANM/EARL harmonization strategies in PET quantification: from daily practice to multicentre oncological studies." *European journal of nuclear medicine and molecular imaging,* Vol. 44pp. 17-31, (2017).

30- Andrea Cozzi *et al.*, "Deep Learning-Based Versus Iterative Image Reconstruction for Unenhanced Brain CT: A Quantitative Comparison of Image Quality." *Tomography,* Vol. 9 (No. 5), pp. 1629-37, (2023).

31- Aziz Makandar and Bhagirathi Halalli, "Image enhancement techniques using highpass and lowpass filters." *International Journal of Computer Applications,* Vol. 109 (No. 14), pp. 12-15, (2015).

32- Sahar Rezaei *et al.*, "The impact of iterative reconstruction protocol, signal-to-background ratio and background activity on measurement of PET spatial resolution." *Japanese journal of radiology,* Vol. 38pp. 231-39, (2020).

33- Alexander E Curtis, Tanya A Smith, Bulat A Ziganshin, and John A Elefteriades, "The mystery of the Z-score." *aorta,* Vol. 4 (No. 04), pp. 124-30, (2016).

34- Haleema Anwar, Qudsia Umaira Khan, Natasha Nadeem, Iqra Pervaiz, Muhammad Ali, and Fatima Fayyaz Cheema, "Epileptic seizures." *Discoveries,* Vol. 8 (No. 2), (2020).

35- Christoph Baumgartner, Johannes P Koren, Martha Britto-Arias, Lea Zoche, and Susanne Pirker, "Presurgical epilepsy evaluation and epilepsy surgery." *F1000Research,* Vol. 8(2019).

36- Nikoletta Pianou and Sofia Chatziioannou, "Imaging with PET/CT in Patients with Epilepsy." in *Epilepsy Surgery and Intrinsic Brain Tumor Surgery*: *Springer*, (2019), pp. 45-50.

37- A Niñerola-Baizán *et al.*, "Relevance of quantification in brain PET studies with 18F-FDG." *Revista Española de*

Medicina Nuclear e Imagen Molecular (English Edition), Vol. 39 (No. 3), pp. 184-92, (2020).

38- Benjamin D Wissel *et al.*, "Prospective validation of a machine learning model that uses provider notes to identify candidates for resective epilepsy surgery." *Epilepsia,* Vol. 61 (No. 1), pp. 39-48, (2020).

39- Antonella Matti, Giacomo Maria Lima, Cinzia Pettinato, Francesca Pietrobon, Felice Martinelli, and Stefano Fanti, "How do the more recent reconstruction algorithms affect the interpretation criteria of PET/CT images?" *Nuclear Medicine and Molecular Imaging,* Vol. 53 (No. 3), pp. 216-22, (2019).

40- Tumelo Carel Godwin Moalosi, "The value of different reconstruction algorithms for quantification of FDG PET brain imaging." *Stellenbosch: Stellenbosch University*, (2016).

41- Charlotte S van der Vos *et al.*, "Quantification, improvement, and harmonization of small lesion detection with state-of-the-art PET." *European journal of nuclear medicine and molecular imaging,* Vol. 44pp. 4-16, (2017).

42- Yu-Jung Tsai, "Penalised image reconstruction algorithms for efficient and consistent quantification in emission tomography." *UCL (University College London)*, (2019).

43- Jie Zhao, Yunfeng Song, Qiong Liu, Shijie Chen, and Jyh-Cheng Chen, "Optimization of the Algorithm for the Implementation of Point Spread Function in the 3D-OSEM Reconstruction Algorithm Based on the List-Mode Micro PET Data." *Electronics,* Vol. 12 (No. 6), p. 1309, (2023).

44- Claudia Kuntner and David Stout, "Quantitative preclinical PET imaging: opportunities and challenges." (in English), *Frontiers in Physics,* Review Vol. 2 (No. 12), 2014-February-28 (2014).

Appendix Tables

Table A2. Calculated relative difference percentage of Z-Scores and SUV$_{max}$ against the reference values. The 336×336 matrix size and 3 mm FWHM Gaussian filter were used for all reconstructions. Δ: relative difference

#iteration×subsets	Pixel size (mm)	RR		non-RR	
		ΔZ-scores	ΔSUV$_{max}$	ΔZ-scores	ΔSUV$_{max}$
1×8	1.01	0.00%	32.41%	10.94%	21.87%
2×8	1.01	14.82%	17.95%	4.14%	10.36%
3×8	1.01	7.41%	12.58%	10.34%	6.28%
2×16	1.01	0.00%	10.66%	10.79%	4.02%
2×21	1.01	14.82%	9.70%	0.00%	3.80%
7×8	1.01	7.41%	5.14%	3.45%	1.49%
3×21	1.01	0.00%	5.14%	3.45%	1.21%
5×16	1.01	7.41%	1.63%	0.00%	0.88%
4×21	1.01	11.11%	3.07%	0.00%	1.10%
5×21	1.01	0.00%	1.68%	6.90%	0.61%
6×21	1.01	7.41%	0.38%	0.00%	0.00%
7×21	1.01	7.41%	0.05%	0.00%	0.17%
8×21	1.01	0.00%	0.00%	0.10%	0.33%
1×8	1.35	3.70%	32.41%	10.34%	21.98%
2×8	1.35	18.52%	18.29%	4.22%	10.19%
3×8	1.35	7.41%	12.82%	3.45%	7.66%
2×16	1.35	11.11%	10.75%	10.34%	5.07%
2×21	1.35	3.70%	10.08%	3.45%	3.64%
7×8	1.35	7.41%	6.10%	0.00%	1.82%
3×21	1.35	11.11%	5.81%	3.45%	1.60%
5×16	1.35	7.41%	2.64%	3.45%	0.44%
4×21	1.35	18.52%	3.36%	6.90%	2.09%
5×21	1.35	3.70%	2.35%	3.45%	1.98%
6×21	1.35	3.70%	1.78%	1.50%	1.27%
7×21	1.35	14.82%	1.63%	0.00%	0.99%
8×21	1.35	11.11%	0.91%	0.00%	0.17%
1×8	2.03	11.11%	32.36%	3.45%	21.54%
2×8	2.03	14.82%	18.15%	4.14%	10.36%
3×8	2.03	11.11%	12.39%	10.94%	5.56%
2×16	2.03	11.11%	10.03%	0.00%	5.23%
2×21	2.03	3.70%	8.59%	0.00%	4.79%
7×8	2.03	3.70%	4.99%	6.90%	2.26%
3×21	2.03	7.41%	4.66%	6.90%	4.08%
5×16	2.03	14.82%	1.63%	3.45%	3.09%
4×21	2.03	11.11%	2.11%	3.45%	3.09%
5×21	2.03	11.11%	0.58%	1.50%	0.22%
6×21	2.03	7.41%	0.91%	1.50%	0.06%
7×21	2.03	3.70%	0.58%	0.00%	0.11%
8×21	2.03	3.70%	0.24%	0.10%	0.83%

Table A3. Calculated relative difference percentage of Z-Scores and SUV$_{max}$ against the reference values. The 336×336 matrix size and 5 mm FWHM Gaussian filter were used for all reconstructions. Δ: relative difference

#iteration×subsets	Pixel size (mm)	RR		non-RR	
		ΔZ-scores	ΔSUV$_{max}$	ΔZ-scores	ΔSUV$_{max}$
1×8	1.01	14.82%	33.94%	10.34%	24.85%
2×8	1.01	18.52%	22.42%	4.14%	14.77%
3×8	1.01	14.82%	17.76%	10.79%	12.29%
2×16	1.01	7.41%	15.94%	3.00%	11.68%
2×21	1.01	7.41%	16.37%	10.94%	10.96%
7×8	1.01	11.11%	14.21%	10.34%	9.15%
3×21	1.01	0.00%	13.83%	6.90%	9.64%
5×16	1.01	3.70%	12.00%	6.90%	8.76%
4×21	1.01	3.70%	13.06%	3.45%	9.31%
5×21	1.01	11.11%	12.63%	10.34%	9.04%
6×21	1.01	3.70%	11.57%	6.90%	9.04%
7×21	1.01	7.41%	11.19%	1.50%	9.15%
8×21	1.01	11.11%	10.95%	1.50%	9.20%
1×8	1.35	3.70%	33.94%	3.45%	25.12%
2×8	1.35	14.82%	22.90%	10.34%	15.37%
3×8	1.35	11.11%	18.29%	10.79%	12.45%
2×16	1.35	14.82%	16.32%	3.00%	11.96%
2×21	1.35	7.41%	16.61%	10.34%	11.24%
7×8	1.35	0.00%	14.88%	3.45%	10.19%
3×21	1.35	14.82%	15.51%	6.90%	10.41%
5×16	1.35	7.41%	12.43%	3.45%	9.70%
4×21	1.35	18.52%	13.59%	6.90%	9.97%
5×21	1.35	7.41%	12.67%	2.00%	9.81%
6×21	1.35	18.42%	11.43%	3.45%	9.59%
7×21	1.35	11.11%	12.05%	1.50%	9.53%
8×21	1.35	7.41%	11.52%	1.50%	9.70%
1×8	2.03	14.82%	33.75%	6.90%	24.57%
2×8	2.03	7.41%	22.71%	10.79%	14.82%
3×8	2.03	3.70%	18.05%	3.45%	11.90%
2×16	2.03	11.11%	15.79%	10.34%	11.96%
2×21	2.03	3.70%	16.42%	6.90%	10.74%
7×8	2.03	3.70%	4.99%	10.94%	9.37%
3×21	2.03	7.41%	14.02%	3.45%	9.59%
5×16	2.03	14.82%	11.81%	6.90%	9.04%
4×21	2.03	3.70%	12.96%	6.90%	8.98%
5×21	2.03	11.11%	11.71%	4.27%	8.71%
6×21	2.03	11.11%	11.38%	6.90%	8.43%
7×21	2.03	7.41%	11.19%	0.20%	8.98%
8×21	2.03	11.11%	10.90%	0.20%	9.09%

Table A4. Calculated relative difference percentage of Z-Scores and SUV$_{max}$ against the reference values. The 336×336 matrix size and 8 mm FWHM Gaussian filter were used for all reconstructions. Δ: relative difference

#iteration×subsets	Pixel size (mm)	RR		non-RR	
		ΔZ-scores	ΔSUV$_{max}$	ΔZ-scores	ΔSUV$_{max}$
1×8	1.01	18.52%	36.97%	10.90%	22.87%
2×8	1.01	11.11%	25.83%	10.90%	22.87%
3×8	1.01	0.00%	26.93%	8.14%	20.77%
2×16	1.01	14.82%	25.49%	10.90%	19.01%
2×21	1.01	3.70%	25.83%	10.90%	19.72%
7×8	1.01	11.11%	25.54%	10.34%	19.17%
3×21	1.01	18.66%	25.68%	6.90%	18.84%
5×16	1.01	7.41%	25.01%	4.14%	18.73%
4×21	1.01	11.11%	25.59%	10.79%	18.40%
5×21	1.01	18.66%	25.25%	4.14%	18.40%
6×21	1.01	7.41%	25.01%	6.90%	18.29%
7×21	1.01	18.66%	24.92%	10.79%	18.46%
8×21	1.01	7.41%	24.96%	10.79%	18.40%
1×8	1.35	19.63%	37.06%	7.00%	28.32%
2×8	1.35	3.70%	30.68%	7.45%	22.98%
3×8	1.35	11.11%	27.56%	10.90%	20.94%
2×16	1.35	18.52%	25.97%	10.90%	19.83%
2×21	1.35	11.11%	26.12%	7.45%	19.78%
7×8	1.35	3.70%	25.68%	10.34%	19.17%
3×21	1.35	7.41%	25.97%	10.34%	18.90%
5×16	1.35	0.00%	25.40%	10.94%	18.84%
4×21	1.35	18.66%	25.83%	10.34%	18.35%
5×21	1.35	0.00%	25.30%	4.25%	18.35%
6×21	1.35	7.41%	25.11%	10.94%	18.57%
7×21	1.35	7.41%	25.01%	6.90%	18.13%
8×21	1.35	3.70%	24.96%	10.94%	18.24%
1×8	2.03	14.82%	37.06%	10.90%	28.15%
2×8	2.03	0.00%	30.92%	10.90%	22.64%
3×8	2.03	11.11%	27.56%	7.45%	20.94%
2×16	2.03	18.52%	25.97%	10.90%	19.67%
2×21	2.03	0.00%	26.31%	7.45%	19.94%
7×8	2.03	18.66%	25.59%	6.90%	19.39%
3×21	2.03	3.70%	25.64%	6.90%	19.06%
5×16	2.03	14.82%	24.92%	10.34%	18.79%
4×21	2.03	17.00%	25.54%	10.79%	18.73%
5×21	2.03	3.70%	24.92%	10.34%	18.62%
6×21	2.03	14.00%	24.77%	10.34%	18.57%
7×21	2.03	11.11%	24.68%	10.34%	18.57%
8×21	2.03	18.42%	24.72%	6.90%	18.51%